



Article

Comparative Analysis of Intelligent Optimization Algorithms for Atmospheric Duct Inversion Using Automatic Identification System Signals

Li-Feng Huang ^{1,2} , Cheng-Guo Liu ^{3,*} , Zhi-Peng Wu ¹, Li-Jun Zhang ², Hong-Guang Wang ², Qing-Lin Zhu ², Jie Han ² and Ming-Chen Sun ²

¹ School of Information Engineering, Wuhan University of Technology, Wuhan 430070, China; huanglf@crirp.ac.cn (L.-F.H.); z.p.wu@whut.edu.cn (Z.-P.W.)

² China Research Institute of Radiowave Propagation, Qingdao 266107, China; zhanglj@crirp.ac.cn (L.-J.Z.); wanghg@crirp.ac.cn (H.-G.W.); zhuql1@crirp.ac.cn (Q.-L.Z.); hanj@crirp.ac.cn (J.H.); sunmc@crirp.ac.cn (M.-C.S.)

³ School of Science, Wuhan University of Technology, Wuhan 430070, China

* Correspondence: liucg@whut.edu.cn

Abstract: Using intelligent optimization algorithms to retrieve atmospheric duct parameters by monitoring automatic identification system (AIS) signals at sea is a new passive remote sensing technology for atmospheric ducts. To thoroughly compare and analyze the inversion results of different intelligent optimization algorithms and optimize the parameters of the algorithms, this study considered a simulated atmospheric duct environment for atmospheric duct inversion using the genetic, simulated annealing, and particle swarm optimization (PSO) algorithms. The results indicated that the PSO algorithm exhibited the best inversion performance. The inversion results of the simulated annealing particle swarm optimization (SAPSO) and PSO algorithms under different inversion parameters were further statistically analyzed, and the atmospheric duct parameters were obtained from measured AIS signals based on the SAPSO algorithm. The inversion results verified the effectiveness of the proposed algorithm, and they continuously improved with additional calculations in the inversion algorithm. However, the changing trend gradually slowed. Therefore, in practical applications, the inversion time consumption should be balanced with the inversion effect to optimize the inversion parameters.

Keywords: atmospheric duct; AIS signal; intelligent optimization; inversion



Citation: Huang, L.-F.; Liu, C.-G.; Wu, Z.-P.; Zhang, L.-J.; Wang, H.-G.; Zhu, Q.-L.; Han, J.; Sun, M.-C. Comparative Analysis of Intelligent Optimization Algorithms for Atmospheric Duct Inversion Using Automatic Identification System Signals. *Remote Sens.* **2023**, *15*, 3577. <https://doi.org/10.3390/rs15143577>

Academic Editors: Zhengqiang Li, Diego Loyola, Mansing Wong, Kai Qin, Zhongwei Huang, Khan Alam and Jing Wei

Received: 26 June 2023
Revised: 11 July 2023
Accepted: 15 July 2023
Published: 17 July 2023



Copyright: © 2023 by the authors. Licensee MDPI, Basel, Switzerland. This article is an open access article distributed under the terms and conditions of the Creative Commons Attribution (CC BY) license (<https://creativecommons.org/licenses/by/4.0/>).

1. Introduction

An atmospheric duct is a nonstandard propagation condition in the troposphere, which causes anomalous propagation; that is, rays bend downwards to the earth surface in a way that is different from the standard, which has a significant impact on the propagation of electromagnetic waves [1,2]. The atmospheric duct can enable long-distance propagation of electromagnetic waves over the horizon, and can also cause the radar system to produce the detection blind area, the clutter echo enhancement, the target-positioning error increase, and other adverse effects, thereby affecting its performance [3–5].

Atmospheric waveguides can be divided into three categories based on their formation mechanisms and spatial distributions: evaporation, surface, and elevated ducts. Surface and elevated ducts can also be collectively referred to as lower atmospheric ducts [6,7]. Evaporation ducts are formed by seawater evaporation in the ocean and attract extensive scientific attention [7]. Researchers have found that lower atmospheric ducts also have a high probability of occurrence, and the affected electromagnetic waves have lower frequencies. Lower atmospheric ducts can have significant impacts on both land and maritime radio systems, therefore receiving increasing attention [3,8].

Traditional lower atmospheric duct measurements typically use radiosondes or sounding rockets to measure meteorological parameters such as atmospheric temperature, relative humidity, and atmospheric pressure at different altitudes, thereby obtaining atmospheric refractive index profiles and diagnosing atmospheric duct parameters [9–11]. This method provides accurate measurements, but it has disadvantages such as inconvenient operation, a high cost, and poor spatial and temporal resolutions. In recent years, researchers have extensively explored the use of remote sensing to detect the atmospheric duct environment, typically by retrieving atmospheric duct parameters through monitoring radar sea clutter or satellite navigation signals [12–15]. Although the inversion accuracy of remote sensing is relatively poor, it has the advantages of convenient operation, high spatiotemporal resolution, continuous monitoring, and regional monitoring, and will remain an important development direction in the future. Using radar sea clutter to retrieve atmospheric ducts is limited in practical applications owing to the need for the radar to be turned on and radiate electromagnetic signals. The retrieval of atmospheric ducts using satellite navigation signals is based on changes in signal power during satellite occultation. Because of limited occultation events, the spatial and temporal resolutions are low.

An automatic identification system (AIS) is a navigation aid system applied to maritime safety and communication between ships and shores and between ships [16,17]. An on-board AIS broadcasts the ship's position, heading, speed, and other information outward at very high frequency (VHF). Owing to the numerous and wide distribution of AIS signal radiation sources at sea, a new passive remote sensing technology for atmospheric ducts is currently used to retrieve lower atmospheric duct parameters by monitoring AIS signals [18–20]. This technology primarily uses intelligent optimization algorithms to search for atmospheric duct profiles and find the set of atmospheric duct parameters that best matches the monitoring data, which is the inversion result. However, many types of intelligent optimization algorithms exist, and thoroughly comparing and analyzing the inversion results of various algorithms and optimizing the parameters of the algorithm are required to more accurately and efficiently use AIS data to retrieve atmospheric duct parameters.

Based on the propagation characteristics of AIS signals and the parabolic equation model, we compare and analyze the atmospheric duct inversion results of different intelligent optimization algorithms using simulation data and further statistically analyze the impact of different inversion parameters on the inversion results. Finally, the atmospheric duct parameters are inverted using measured AIS data to verify the reliability of the inversion method.

2. Theory and Method

2.1. AIS Signal Propagation Characteristics

The frequency of the AIS signal is $162 \text{ MHz} \pm 25 \text{ kHz}$; that is, 161.975 MHz and 162.025 MHz. Because these two frequencies are adjacent and no significant difference exists in the propagation characteristics, the frequency of the AIS signal can be regarded as approximately 162 MHz in the calculation of radio wave propagation. It is well-known that the evaporation duct only affects frequencies above 1 GHz, whereas the lower atmospheric duct may affect AIS signals. When the lower atmospheric duct satisfies certain conditions, it can trap the AIS signal on the sea surface and generate over-the-horizon propagation.

The parabolic equation (PE) model is a parabolic approximation of the Helmholtz wave equation. It is useful for studying the abnormal propagation of electromagnetic waves in complex environments, such as atmospheric ducts, and is easy to implement on computers. Therefore, it is widely used to calculate the radio wave propagation loss [21–24]. The following is the basic model equation [25–27]:

$$\frac{\partial u(x, z)}{\partial x} = \frac{ik_0}{2} \left[\frac{1}{k_0^2} \frac{\partial^2}{\partial z^2} + n^2(x, z) - 1 \right] u(x, z) \quad (1)$$

where $u(x, z)$ is the electric- or magnetic-field component, k_0 is the wavenumber, and $n(x, z)$ is the atmospheric refractive index at various distances and heights.

Owing to the considerable differences in the propagation path and path loss of electromagnetic signals in different environments, the atmospheric modified refractive index profiles in evaporation duct and lower atmospheric duct environments were simulated. The parameters of the AIS signals and atmospheric modified refractive index profile were substituted into the PE model to simulate the propagation path and path loss of the AIS signal in different atmospheric duct environments. Then, the effects of evaporation duct and lower atmospheric duct environments on AIS signal propagation were simulated.

Figure 1 shows the simulated atmosphere-modified refractive index profile and the AIS signal propagation loss variation diagram. We considered a height of the evaporation duct of 30 m, a lower atmospheric duct height of 150 m, and a duct strength of 20 M.

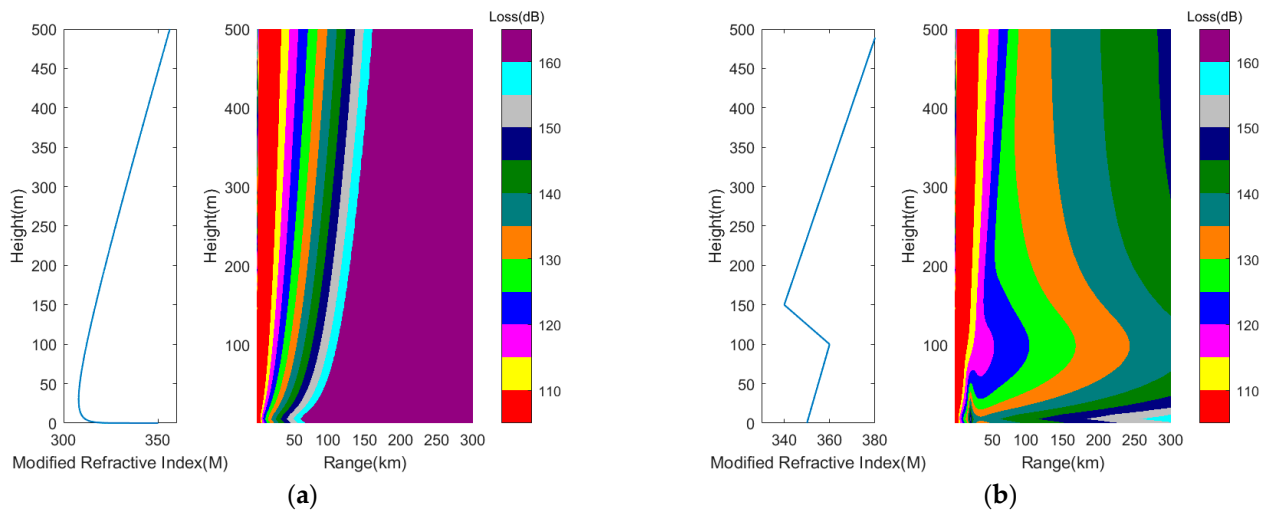


Figure 1. Atmospheric modified refractive index profiles and AIS signal propagation loss diagram. (a) Evaporation duct; (b) lower atmospheric duct.

As shown in Figure 1, the AIS signal propagates normally in the evaporation duct environment, whereas there is a considerable abnormal propagation in the lower atmospheric duct environment; that is, the lower atmospheric duct has a significant impact on the propagation of AIS signals. An onboard AIS signal contains information such as the longitude, latitude, heading, and speed of the ship. The positions of the different ships can be obtained by receiving the AIS signals, thereby obtaining the power intensity of the AIS signal in different directions and distances. Therefore, the AIS signal can be used to retrieve the environmental parameters of the lower atmospheric duct. The AIS horizon and over-the-horizon signals received by the shore-based AIS antenna are shown in Figure 2.

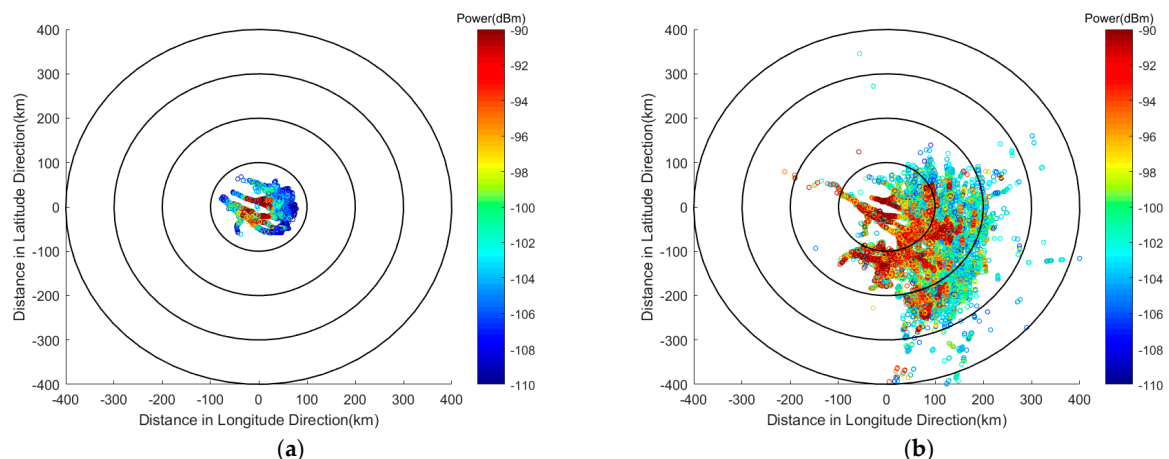


Figure 2. Comparison diagram of AIS horizon signals and over-the-horizon signals. (a) AIS horizon signals; (b) AIS horizon and over-the-horizon signals.

2.2. Atmospheric Duct Parameterization

An atmospheric duct is an abnormal atmospheric structure in the troposphere, and its atmospherically modified refractive index gradient satisfies the following equation [1]:

$$dM/dz < 0 \quad (2)$$

where z is the altitude and M is the modified refractive index. Figure 3 shows the modified refractive index profiles corresponding to different types of lower atmospheric ducts [2].

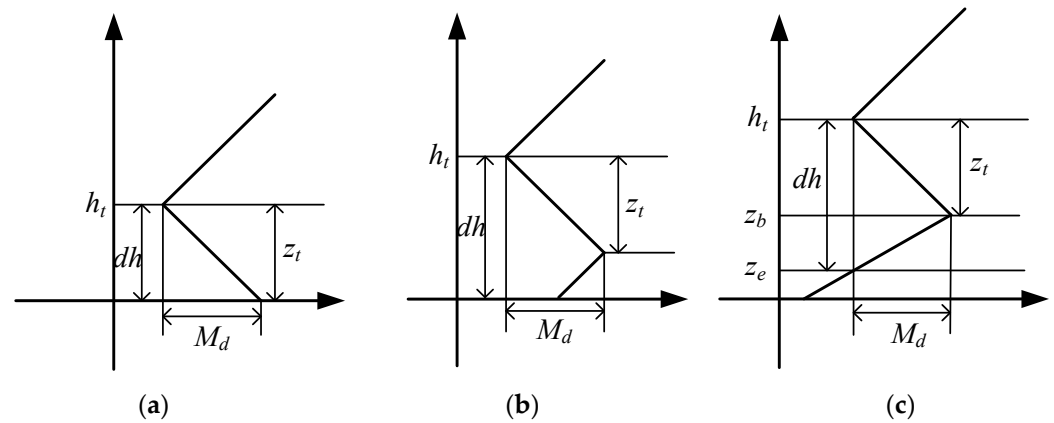


Figure 3. Modified refractive index profiles of lower atmospheric duct. (a) Surface duct; (b) surface-based duct; (c) elevated duct.

In Figure 3, h_t is the duct top height in meters, dh is the duct thickness in meters, M_d is the duct strength in M units, z_b is the bottom height of the duct layer in meters, z_t is the duct layer thickness in meters, and z_e is the duct bottom height in meters.

As shown in Figure 3, the lower atmospheric duct parameters can be uniformly simplified into a four-parameter model, which can be approximated using a trilinear profile model [12]:

$$M(z) = M_0 + \begin{cases} cz & \text{for } z \leq z_b \\ cz_b - \frac{M_d}{z_t}(z - z_b) & \text{for } z_b < z \leq z_b + z_t \\ cz_b - M_d + 0.118(z - z_b - z_t) & \text{for } z > z_b + z_t \end{cases} \quad (3)$$

where $M(z)$ is the atmospheric modified refractive index at altitude z in M units, M_0 is the atmospheric modified refractive index of the surface or sea surface, generally considered as 350, z is the height in meters, and c is the slope of the bottom layer in M units per meter. Determining the values of c , z_b , z_t , and M_d yields lower atmospheric duct profiles. Therefore, the lower atmospheric duct parameters retrieved from the AIS signals provided c , z_b , z_t , and M_d .

2.3. Basic Inversion Method

An intelligent optimization algorithm is a search process or rule based on certain ideas and mechanisms to obtain the solution to a problem that meets specific requirements through certain rules. The steps for retrieving the lower atmospheric duct using AIS signals based on the optimization algorithm are shown in Figure 4.

1. Preprocess measures AIS data to generate AIS path propagation loss;
2. Generate parameterized profiles of atmospheric ducts using intelligent optimization algorithms;
3. Based on AIS parameters and atmospheric duct parameterized profiles, calculate the propagation loss data of the AIS using the PE model;
4. Establish an objective function to calculate the matching degree between the simulated AIS and measured loss data;

5. Use the intelligent optimization algorithm to search for atmospheric duct profile parameters and repeat steps 2–4;
6. When the maximum number of iterations is reached or the objective function value meets the requirements, obtain the set of atmospheric duct profile parameters with the highest matching degree and construct the lower atmospheric duct profile, which is the optimal one.

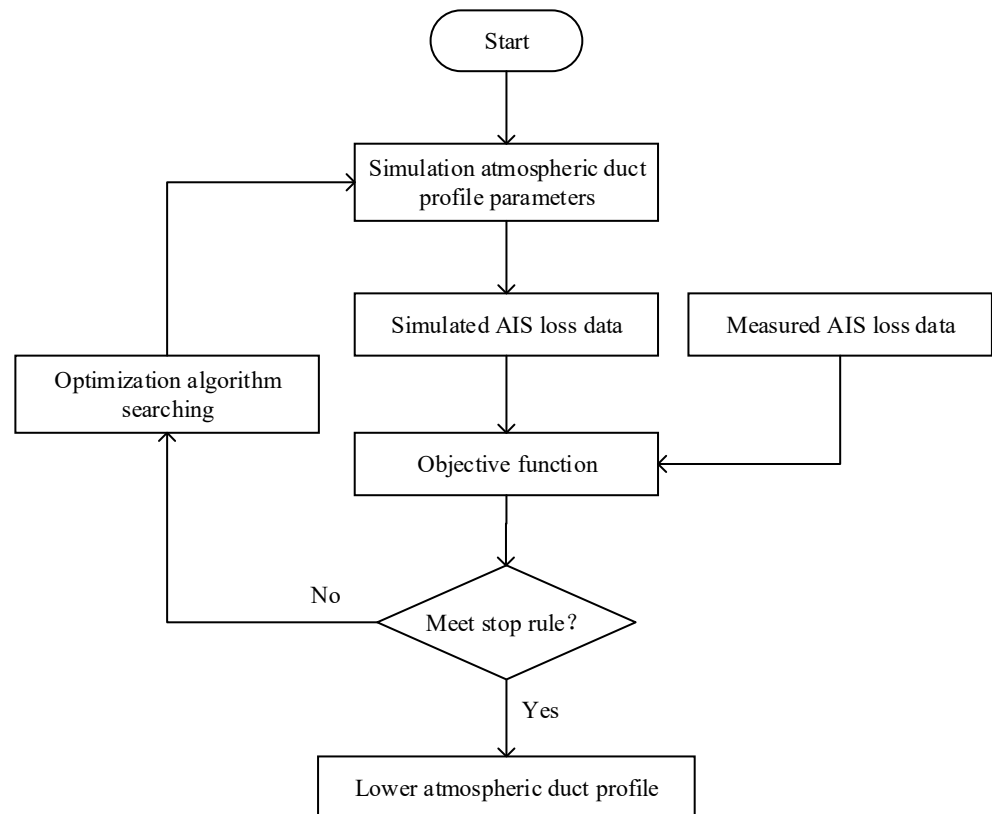


Figure 4. AIS signal inversion for lower atmospheric duct.

The objective function was primarily used to evaluate the matching degree between the simulated AIS signal and measured loss data. We use

$$f(x) = e^T e / L \quad (4)$$

$$e = P_c^{obs} - P_c^{sim} \quad (5)$$

where P_c^{obs} and P_c^{sim} are the AIS-measured and PE-model-calculated loss data, respectively, and L is the length of P_c^{obs} . A smaller value of $f(x)$ indicates a higher degree of matching of the inversion results. When $f(x)$ satisfies the termination condition or the algorithm reaches the maximum number of iterations, the inversion results are retrieved. The inversion result in this study was a single approximate atmospherically modified refractive index profile, equivalent to the profile of the AIS signal propagation path, which differs from sounding and provides a vertical profile.

3. Intelligent Optimization Algorithm Inversion

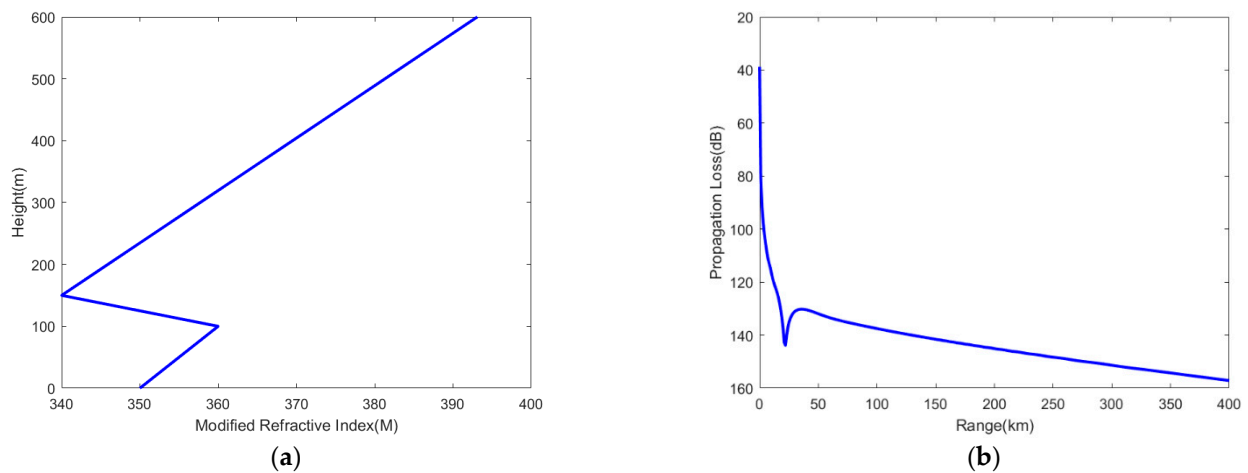
3.1. Inversion Parameter Settings

To facilitate a comparative analysis of the accuracy of the inversion results using intelligent optimization algorithms, a lower atmospheric duct profile was simulated as a measured profile with the parameters listed in Table 1.

Table 1. Simulated lower atmospheric duct profile parameters.

Parameter	Value
Slope of bottom layer (c)	0.1 M unit/m
Bottom height of duct layer (z_b)	100 m
Thickness of duct layer (z_t)	50 m
Duct strength (M_d)	20 M unit

Assuming that the height of the AIS transmitting antenna was 15 m and the height of the receiving antenna was 18 m, the AIS signal path propagation loss simulated based on the PE model was considered as the measured loss. The simulated atmospheric duct profile and path propagation loss diagram are shown in Figure 5.

**Figure 5.** Simulated atmospheric duct profile and path propagation loss. (a) Atmospheric duct profile; (b) path propagation loss of AIS signal.

The boundary settings for the lower atmospheric duct parameters in the inversion algorithm are listed in Table 2.

Table 2. Limits of lower atmospheric duct parameters.

Parameter	Minimum	Maximum
c (M Unit/m)	0	0.2
z_b (m)	0	400
z_t (m)	1	100
M_d (M Unit)	1	80

3.2. Genetic Algorithm

The genetic algorithm (GA) was proposed by Holland in 1975 as an adaptive global optimization probability search algorithm that simulates the genetic and evolutionary processes of living organisms in natural environments [28–30]. The core of the GA consists of three steps: selection, exchange, and mutation. A basic flowchart of the algorithm is shown in Figure 6.

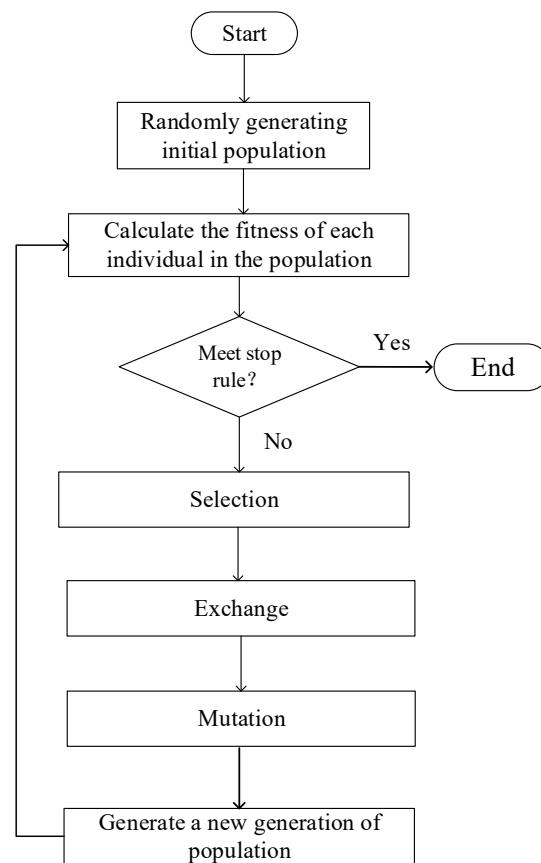


Figure 6. Basic flowchart of GA.

For the parameters of GA, a generation gap determines the degree of change in the selection of each generation, generally between 0.1 and 1.0. The exchange rate determines the number of individuals crossing in each generation, generally between 0.4 and 1.0. The mutation rate determines the number of individuals undergoing mutation in each generation, generally between 0.001 and 0.1. The parameter settings for the GA in this study are listed in Table 3 [31].

Table 3. Parameters of GA.

Parameter	Value
Genetic algebra	20
Population size	20
Generation gap	0.95
Exchange rate	0.7
Mutation rate	0.01

The parameters of the lower atmospheric duct retrieved using the GA are listed in Table 4. The inversion results in Figure 7 indicate that the GA can retrieve the parameters of the lower atmospheric duct.

Table 4. Lower atmospheric duct parameters retrieved by GA.

Parameter	Simulated True Value	Inverted Value
c (M Unit/m)	0.1	0.167
z_b (m)	100	121.7
z_t (m)	50	2.3
M_d (M Unit)	20	28.2

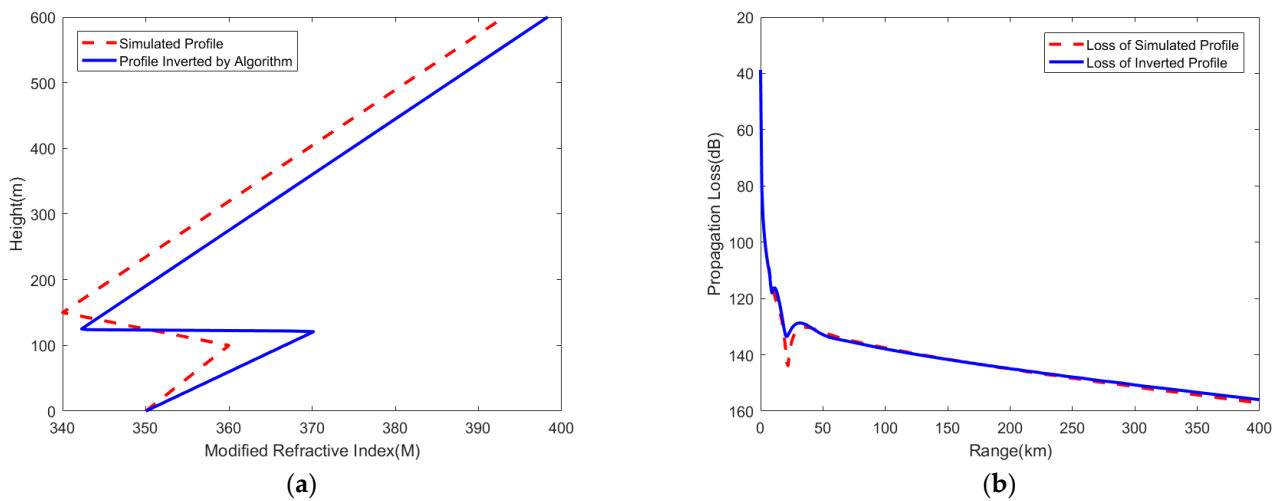


Figure 7. GA inversion results. (a) Atmospheric duct profile; (b) path propagation loss of AIS signal.

3.3. Simulated Annealing Algorithm

The simulated annealing (SA) algorithm was proposed by Metropolis in 1953 to simulate the crystallization of solid matter in statistical physics [32]. The SA algorithm compares the optimization problem with the annealing process. The basic process of the SA algorithm is shown in Figure 8.

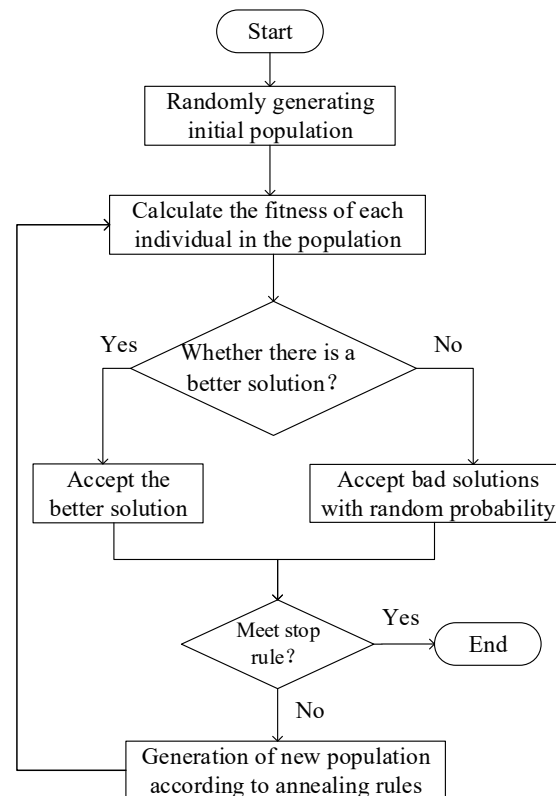


Figure 8. Basic flowchart of SA algorithm.

For the parameters of the SA algorithm, the initial temperature refers to the temperature at the beginning of the algorithm, generally between 100 and 1000. The temperature attenuation coefficient is the speed of temperature reduction in the algorithm, which is generally between 0.5 and 0.99. The parameter settings for the SA algorithm in this study are listed in Table 5 [33].

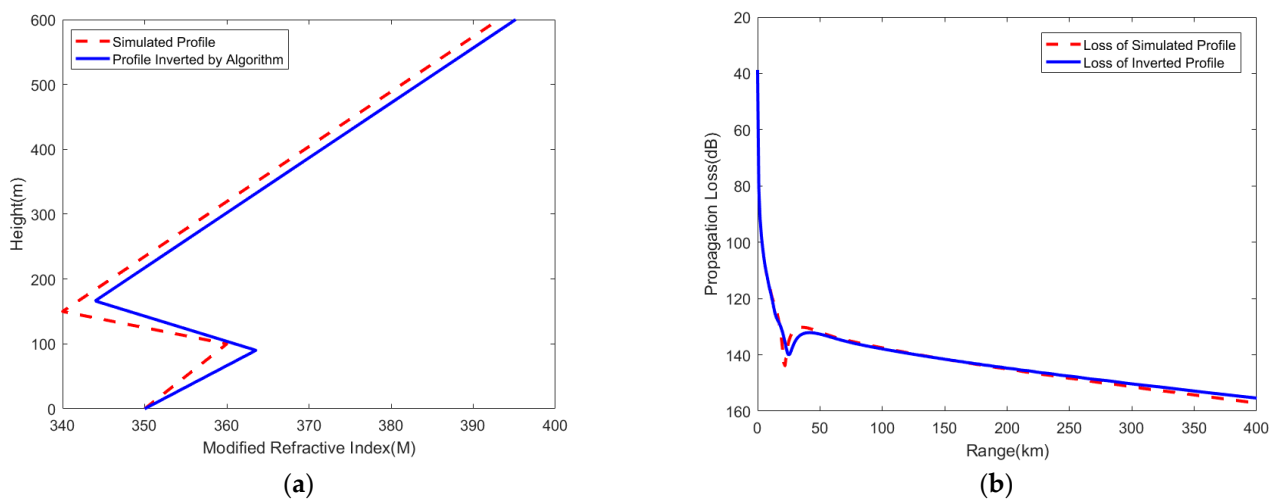
Table 5. Parameters of SA algorithm.

Parameter	Value
Maximum number of iterations	20
Iterations per temperature	20
Initial temperature	100
Temperature attenuation coefficient	0.95

The parameters of the lower atmospheric duct retrieved using the SA algorithm are listed in Table 6. The inversion results in Figure 9 demonstrate that the SA algorithm can better retrieve the parameters of the lower atmospheric duct.

Table 6. Lower atmospheric duct parameters retrieved by SA algorithm.

Parameter	Simulated True Value	Inverted Value
c (M Unit/m)	0.1	0.15
z_b (m)	100	90.1
z_t (m)	50	76.1
M_d (M Unit)	20	19.6

**Figure 9.** SA algorithm inversion results. (a) Atmospheric duct profile; (b) path propagation loss of AIS signal.

3.4. Particle Swarm Optimization Algorithm

The particle swarm optimization (PSO) algorithm was proposed by Kennedy and Eberhart in 1995 and is based on the foraging behavior of birds [34]. The algorithm is based on population iterations, where the population follows the optimal particle to search the solution space. The basic process of the algorithm is shown in Figure 10.

Based on the elementary PSO algorithm, Shi et al. proposed an improved algorithm with a linearly decreasing inertia factor w [35], which enables the algorithm to have greater search ability at the initial stage of the search and can obtain more accurate results at a later stage.

For the parameters of the PSO algorithm, the individual learning factor and the social learning factor adjust the maximum step size of flying in the direction of the individual best particle and the global best particle, respectively, which are generally about 2.0. The maximum and minimum inertia factors represent the maximum and minimum values of the linearly decreasing inertia factor, respectively. The parameter settings for the PSO algorithm in this study are listed in Table 7 [36,37].

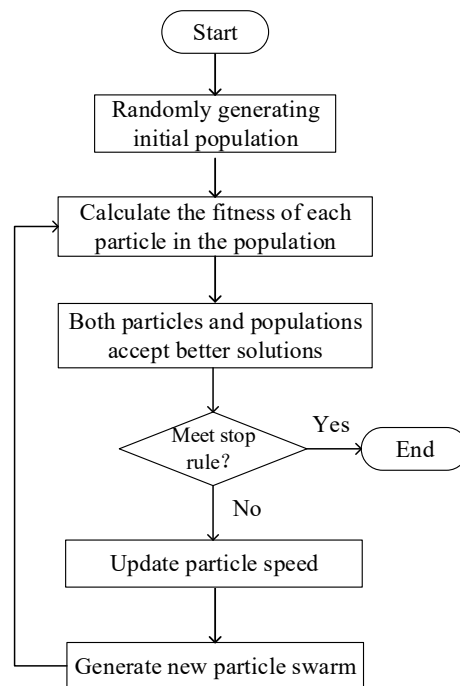


Figure 10. Basic flowchart of PSO algorithm.

Table 7. Parameters of PSO algorithm.

Parameter	Value
Maximum number of iterations	20
Number of particles	20
Individual learning factor	2
Social learning factor	2
Maximum inertia factor	0.9
Minimum inertia factor	0.4

The parameters of the lower atmospheric duct retrieved using the PSO algorithm are listed in Table 8. The inversion results in Figure 11 demonstrate that the PSO algorithm can better retrieve the parameters of the lower atmospheric duct.

Table 8. Lower atmospheric duct parameters retrieved by PSO algorithm.

Parameter	Simulated True Value	Inverted Value
c (M Unit/m)	0.1	0.11
z_b (m)	100	120.1
z_t (m)	50	17.0
M_d (M Unit)	20	22.9

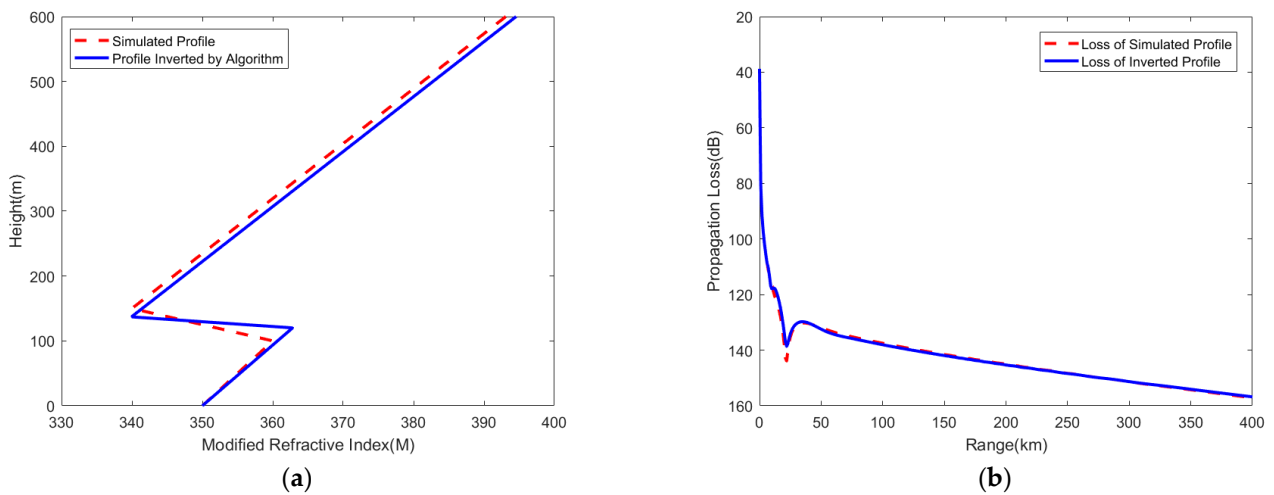


Figure 11. PSO algorithm inversion results. (a) Atmospheric duct profile; (b) path propagation loss of AIS signal.

3.5. Comparative Analysis of Inversion Results

Owing to the uncertainty of the results obtained from each inversion of the intelligent optimization algorithms, to better compare and analyze the effectiveness of each intelligent optimization algorithm in the AIS signal inversion of the atmospheric duct, the three evaluated algorithms were used for 100 times. The optimal objective function values for each inversion of the three algorithms are shown in Figure 12.

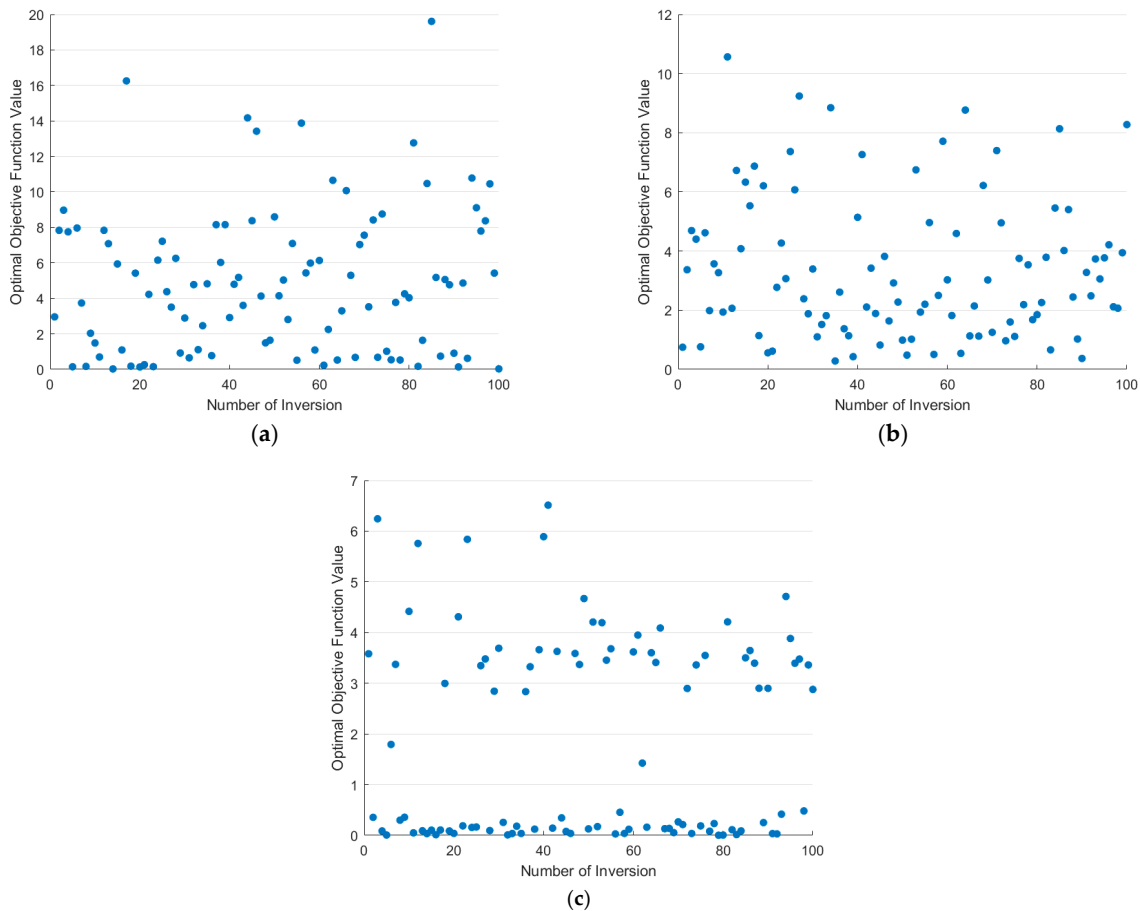


Figure 12. Optimal objective function values obtained from inversion using three intelligent optimization algorithms. (a) GA; (b) SA algorithm; (c) PSO algorithm.

The inversion results of the three intelligent optimization algorithms using the AIS signal for the atmospheric duct are ranked as follows: PSO algorithm, SA algorithm, and GA. The average values of the optimal objective function retrieved 100 times by the three algorithms were calculated to be 1.84, 3.33, and 4.83 for the PSO algorithm, SA algorithm, and GA, respectively.

To compare and analyze the accuracy of the inversion results of three intelligent optimization algorithms more deeply, a set of elevated duct profiles was simulated as a measured profile with the parameters listed in Table 9.

Table 9. Simulated elevated duct profile parameters.

Parameter	Value
Slope of bottom layer (c)	0.15 M unit/m
Bottom height of duct layer (z_b)	80 m
Thickness of duct layer (z_t)	60 m
Duct strength (M_d)	8 M unit

The simulated elevated duct profile and path propagation loss diagram are shown in Figure 13.

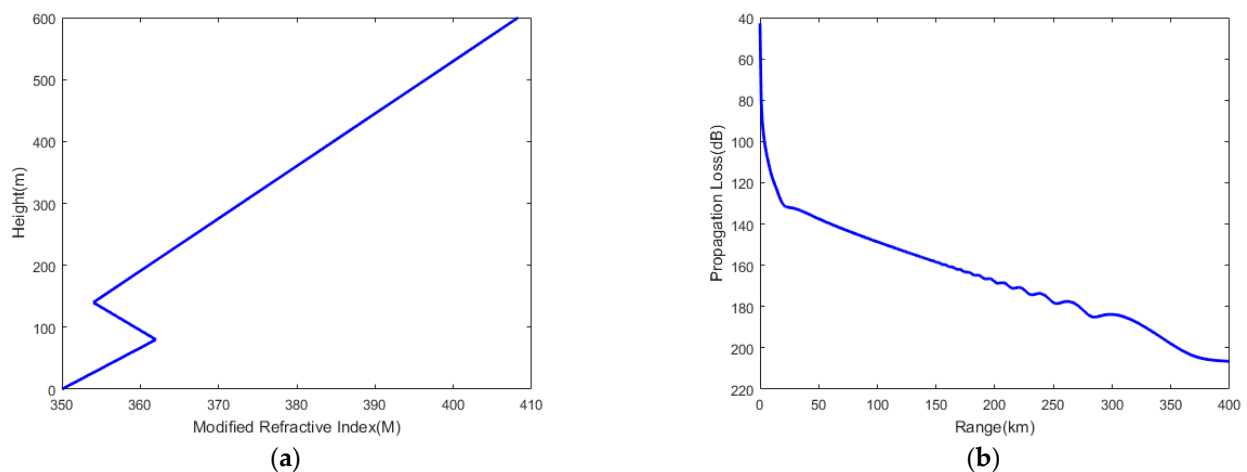


Figure 13. Simulated elevated duct profile and path propagation loss. (a) Elevated duct profile; (b) path propagation loss of AIS signal.

The three intelligent optimization algorithms were used to invert the above atmospheric duct parameters 100 times. The optimal objective function values per inversion using the three algorithms are shown in Figure 14.

The average optimal objective functions retrieved 100 times were 7.28, 8.05, and 15.00 for the PSO algorithm, SA algorithm, and GA, respectively, which are consistent with the rankings of the inversion results of the previous group. The PSO algorithm has a positive effect on the AIS data inversion of the atmospheric duct.

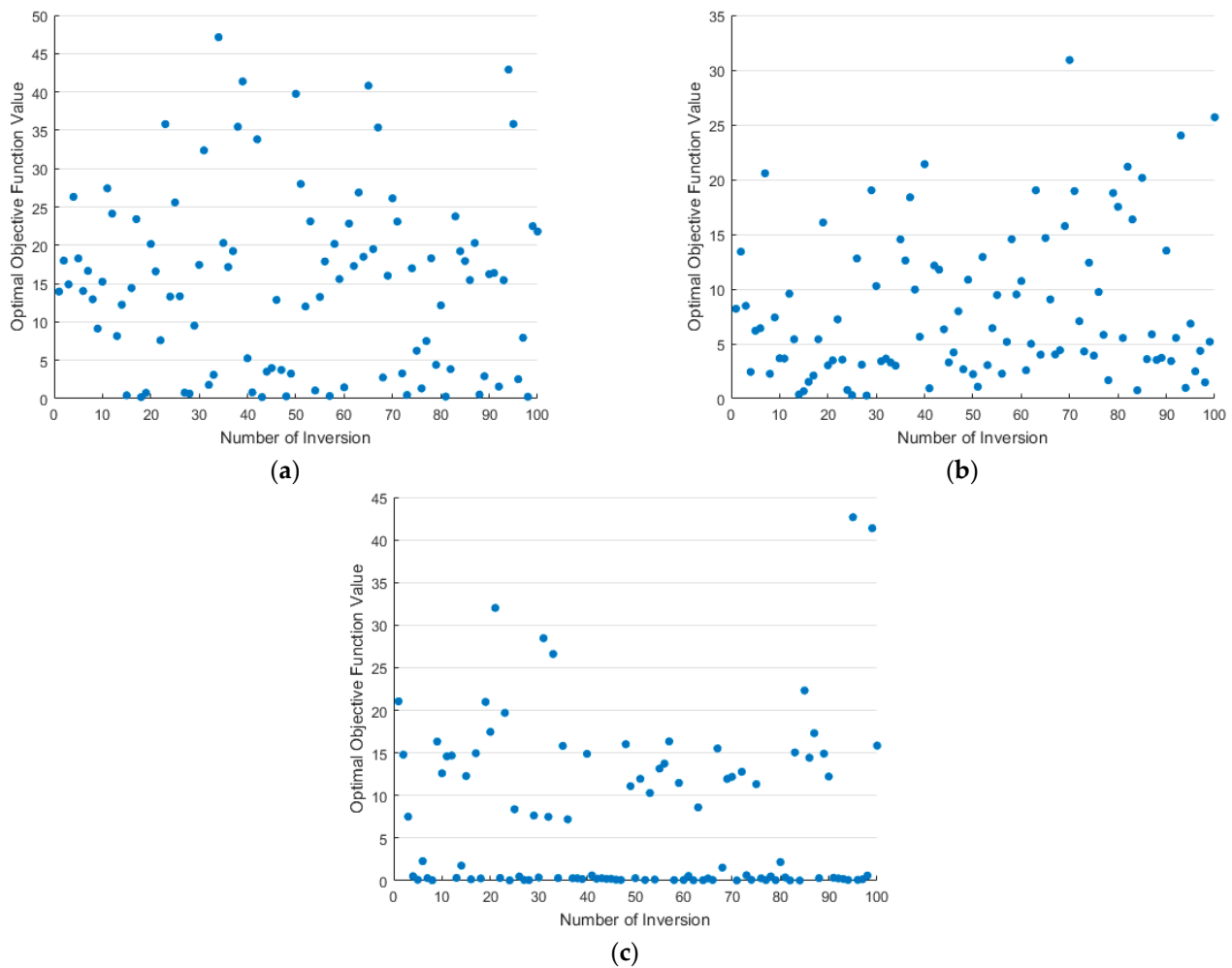


Figure 14. Optimal objective function values obtained from inversion using three intelligent optimization algorithms. (a) GA; (b) SA algorithm; (c) PSO algorithm.

4. Comparative Analysis of Inversion Results Using Combined Algorithms

4.1. Simulated Annealing Particle Swarm Optimization Algorithm

The above analysis demonstrates that the PSO algorithm has a better effect based on the AIS data inversion of the atmospheric duct. However, as shown in Figure 12c, the objective function values of the PSO algorithm are primarily concentrated near zero and four. According to the inversion principle of the PSO algorithm, when the objective function value is near zero, the inversion result is close to the global optimum. In contrast, when the objective function value is near four, the inversion result is trapped in a local optimum. The inversion result of the SA algorithm is inferior only to that of the PSO algorithm, and it can accept a bad solution with a certain probability; that is, it can jump out of a local optimum with a certain probability. Therefore, the SA and PSO algorithms can be combined to retrieve atmospheric duct parameters. The simulated annealing particle swarm optimization (SAPSO) algorithm is based on the PSO algorithm, and SA is added at a later stage to accept bad solutions with a certain probability, ensuring rapid convergence of the inversion algorithm and reducing the probability of falling into a local optimum. The basic process of the SAPSO algorithm is shown in Figure 15.

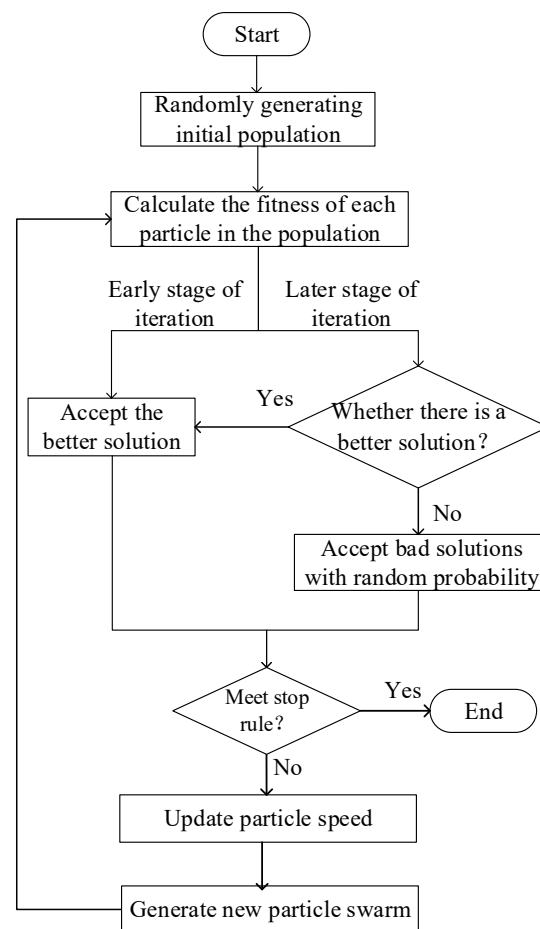


Figure 15. Basic flowchart of the SAPSO algorithm.

Based on the parameter settings of the SA algorithm and PSO algorithm mentioned above, the parameter settings for the SAPSO algorithm are listed in Table 10.

Table 10. Parameters of SAPSO algorithm.

Parameter	Value
Maximum number of iterations	20
Number of particles	20
Individual learning factor	2
Social learning factor	2
Maximum inertia factor	0.9
Minimum inertia factor	0.4
Initial temperature	100
Temperature attenuation coefficient	0.95

The parameters of the lower atmospheric duct retrieved using the SAPSO algorithm are listed in Table 11. The inversion results in Figure 16 demonstrate that the SAPSO algorithm can retrieve accurate parameters of the lower atmospheric duct.

Table 11. Lower atmospheric duct parameters retrieved by SAPSO algorithm.

Parameter	Simulated True Value	Inverted Value
c (M Unit/m)	0.1	0.16
z_b (m)	100	103.7
z_t (m)	50	42.0
M_d (M Unit)	20	22.6

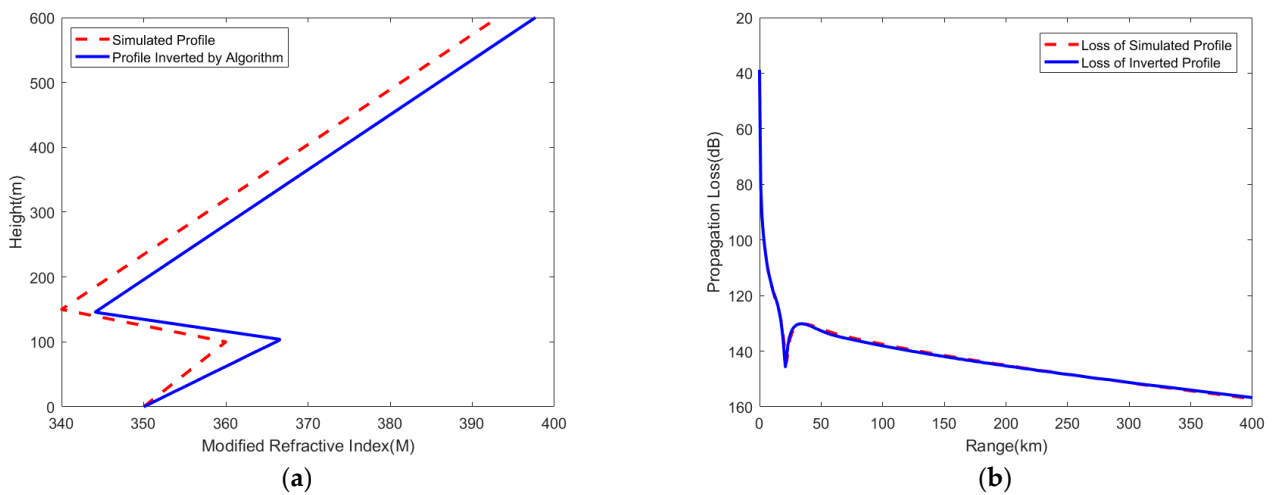


Figure 16. SAPSO algorithm inversion results. (a) Atmospheric duct profile; (b) path propagation loss of AIS signal.

4.2. Comparative Analysis of SAPSO and PSO Inversion Results

SAPSO was used to perform 100 atmospheric duct inversions, and the optimal objective function values for each inversion are shown in Figure 17.

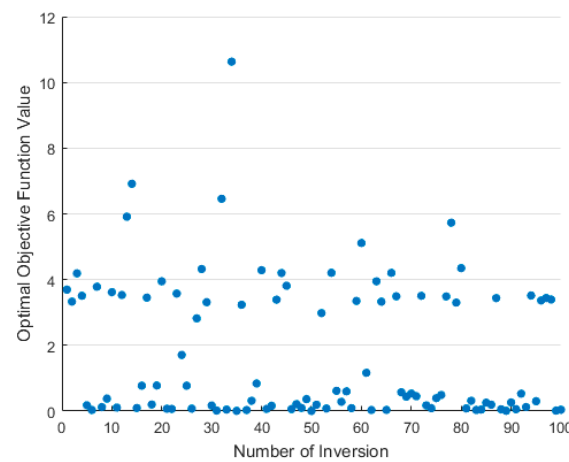


Figure 17. Optimal objective function values of SAPSO algorithm inversion.

Based on the statistics, the average value of the optimal objective function value retrieved 100 times by the SAPSO algorithm is 1.80, and the result of the PSO algorithm (Figure 12) is 1.84; that is, the inversion effects of the two optimization algorithms are equivalent.

To thoroughly compare and analyze the inversion effects of the PSO and SAPSO algorithms, 500 inversion tests were conducted using the two algorithms under different numbers of iterations and population sizes, and the optimal objective function values were averaged. The results are presented in Table 12.

Table 12. Average of optimal objective function values under different inversion parameters.

Population Size	Number of Iterations for PSO				Number of Iterations for SAPSO			
	10	20	30	40	10	20	30	40
10	3.69	2.34	2.47	2	3.56	2.51	2.26	2.09
20	2.35	1.74	1.38	1.37	2.3	1.7	1.56	1.37
30	1.95	1.19	1.01	0.99	1.67	1.32	1.08	1.14
40	1.69	1.04	0.86	0.7	1.46	1.06	1.06	0.84
50	1.34	0.91	0.73	0.71	1.15	0.83	0.77	0.75

As shown in Table 12, both the PSO and SAPSO algorithms have optimal objective function values that decrease with more iterations or larger populations. This is consistent with the theory of optimization algorithms. Thus, more iterations and larger populations improve the optimization inversion results. However, the corresponding calculation times also increase.

Figure 18 compares the PSO and SAPSO inversion results at different numbers of iterations. When the number of iterations is 10, the inversion result of SAPSO is slightly better than that of PSO. When the number of iterations is 20, the inversion results for SAPSO and PSO are equivalent. When the number of iterations is 30 or 40, the inversion results of PSO are slightly better than those of SAPSO.

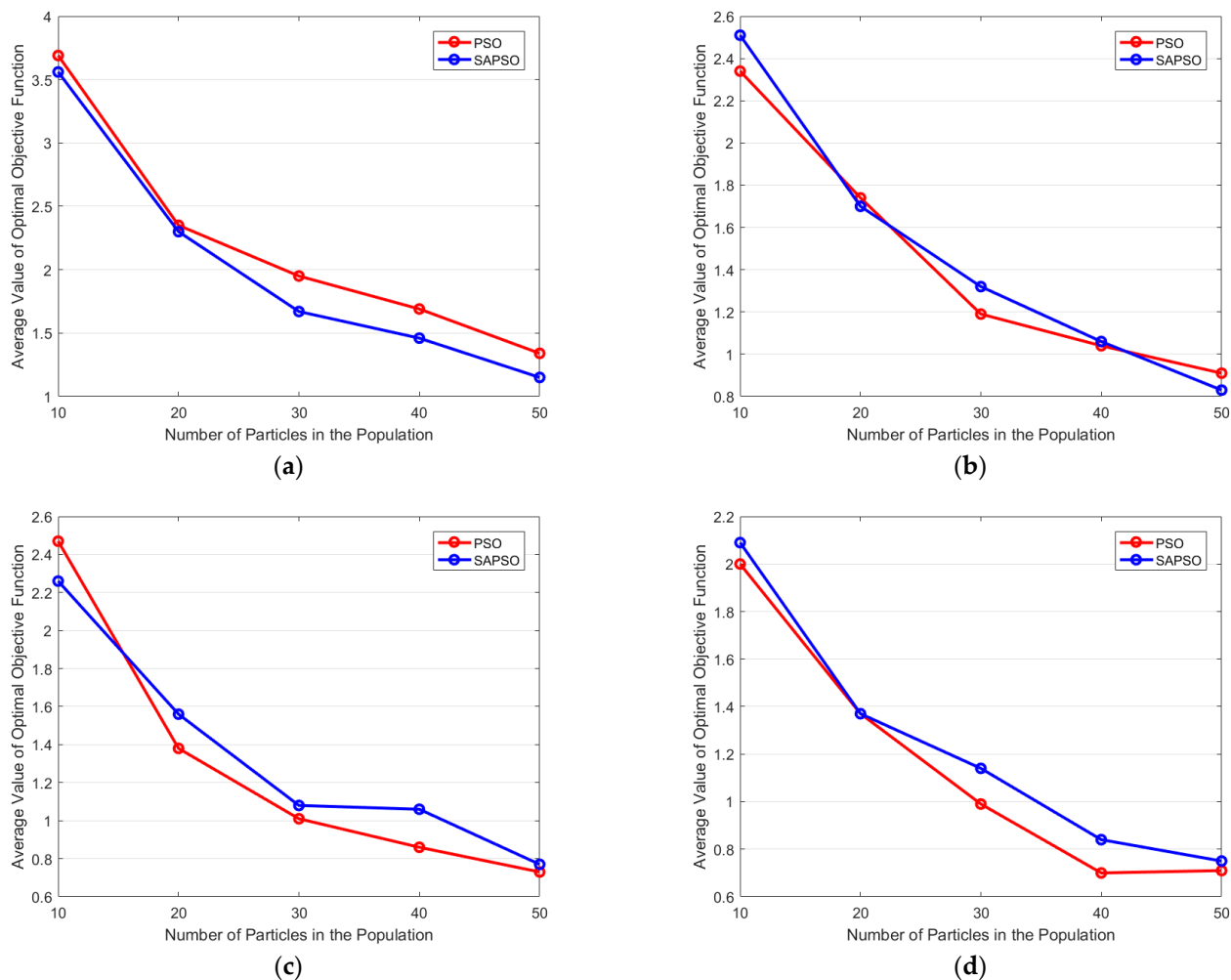


Figure 18. Comparison of PSO and SAPSO inversion results under different numbers of iterations. (a) 10; (b) 20; (c) 30; and (d) 40 iterations.

From the above comparative results, the actual inversion effect of the SAPSO algorithm does not demonstrate significant theoretical advantages. The reasons for this outcome may be related to two points. (1) The number of iterations in the inversion is relatively small, which cannot demonstrate the advantages of the algorithm. (2) The objective function is relatively complex, which affects the inversion performance of the algorithm.

From the statistical results, more iterations and larger populations improve inversion, but the inversion effect and number of calculations should be comprehensively considered in practical applications owing to the long calculation time of the PE model for inversion. Based on the optimization algorithm rules, the inversion calculation of the initial population must be performed before the algorithm begins its iterative process. Therefore, the total number of calculations for inversion is given by

$$N = n * (K + 1) \quad (6)$$

where N is the number of calculations, n is the population size, and K is the number of iterations.

Based on the statistical results in Table 12, Figure 19 presents the inversion results of PSO and SAPSO for different numbers of calculations.

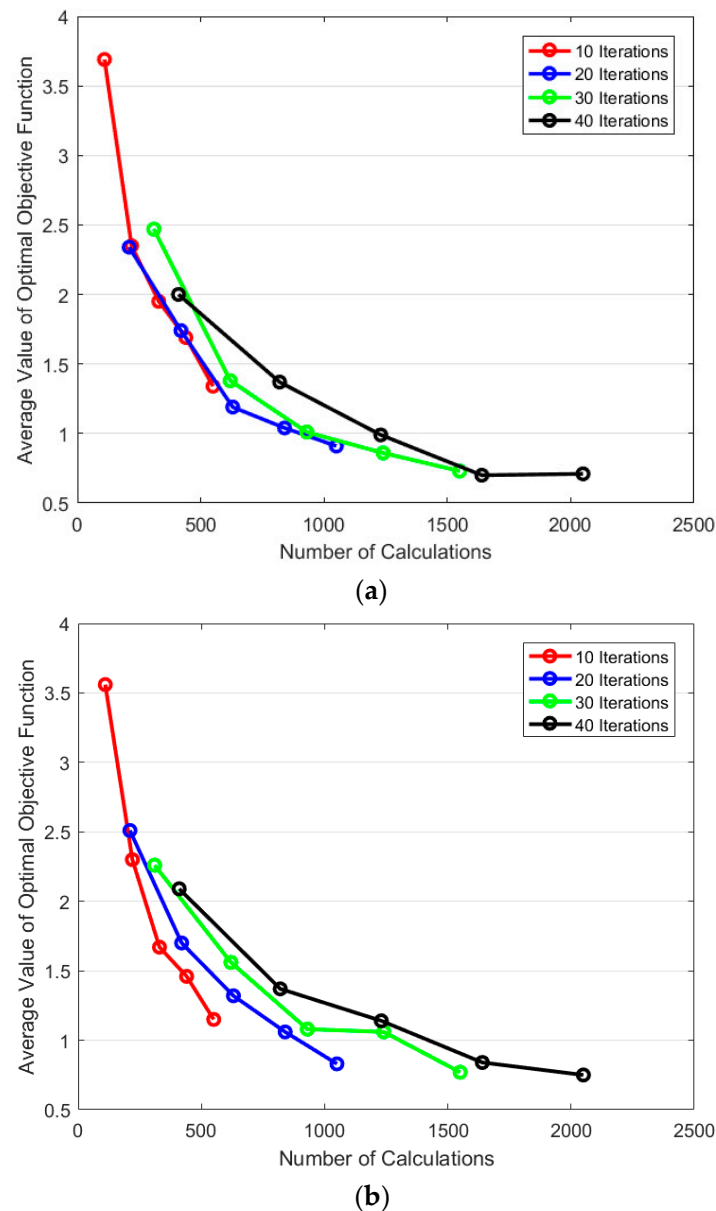


Figure 19. Inversion results under different numbers of calculations. (a) PSO algorithm; (b) SAPSO algorithm.

As shown in Figure 19, for PSO or SAPSO, when the number of calculations is the same, fewer iterations provide better optimization results. As the number of calculations increase, the results of the optimized inversion improve, but the change trend gradually slows.

Therefore, when using AIS data to invert atmospheric duct parameters based on intelligent optimization algorithms, the optimization algorithm, number of iterations, and population size should be properly selected based on the limitations of inversion time. Based on the above inversion results, when the inversion time is sufficient, the PSO algorithm with 30 iterations and 50 particles in the population is suitable. Additional iterations can be performed when time permits. When the inversion time is limited, the SAPSO algorithm with 10 iterations and 50 particles can be used.

4.3. Inversion of Measured AIS Data

Based on the analysis results above, the parameters listed in Table 13 were selected for the atmospheric duct inversion of the measured AIS data.

Table 13. Selected parameters for inversion using measured AIS data.

Parameter	Value
Inversion algorithm	SAPSO
Maximum number of iterations	10
Number of particles	50
Individual learning factor	2
Social learning factor	2
Maximum inertia factor	0.9
Minimum inertia factor	0.4
Initial temperature	100
Temperature attenuation coefficient	0.95

We installed AIS receiving antennas along the coast of Shanghai, China, and conducted AIS signal reception experiments. Figure 20 shows the distance–time and distance–azimuth distributions of the AIS signal power as collected on 4 October 2021.

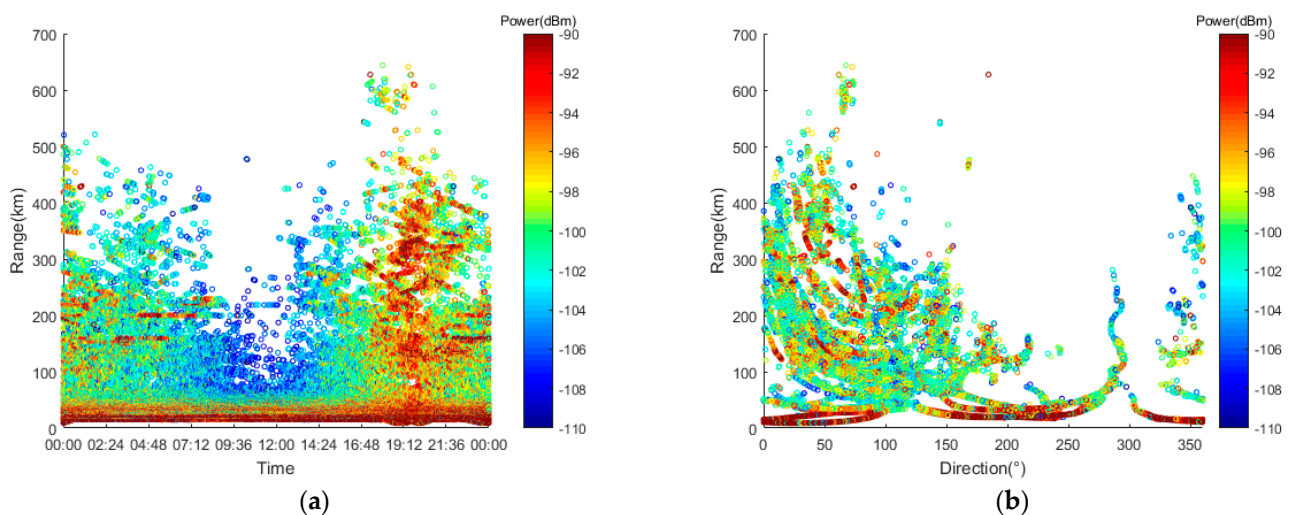


Figure 20. Measured AIS signal power data from 4 October 2021. (a) Distance–time distribution; (b) distance–azimuth distribution.

Figure 20 shows that a significant over-the-horizon phenomenon in the AIS signal received on that day occurred, and significant differences occurred in the maximum distance and power of the AIS signal at different times and directions. Hence, a strong atmospheric duct environment occurred on that day, and the atmospheric environment varied at different times and in different directions. Around 19:00 or at an approximate direction of 60° , the AIS signal had the farthest distance and strongest signal power. Thus, the inversion of atmospheric duct parameters was performed using AIS data at 19:00 and 60° , obtaining the inversion results shown in Figure 21.

As shown in Figure 21a, a particularly strong lower atmospheric duct exists at this time and direction, and the slope of the bottom layer is 0.077 M/m, the bottom height of the duct layer is 353.9 m, the thickness of the duct layer is 100 m, and the duct strength is 39.2 M. As shown in Figure 21b, the power calculated by the inversion profile is consistent with the power measured by the AIS, verifying the effectiveness of the inversion algorithm.

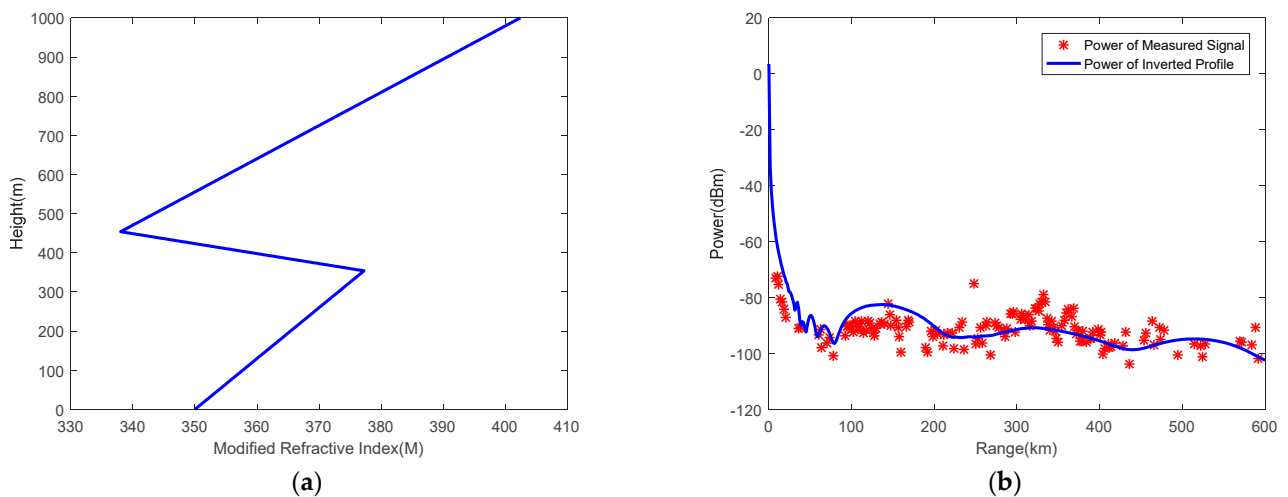


Figure 21. Inversion results using AIS measured data at 19:00 and 60°. (a) Inverted atmospheric duct profile; (b) comparison of measured signal power and inverted profile calculation power.

As shown in Figure 21b, a deviation remains between the AIS inversion power and measured power. The reasons for this phenomenon may include the following three points. (1) As the measured AIS signals were transmitted by different ships, there may be some differences in the transmission power itself, which was not uniform. (2) The number of inversion iterations was relatively small, and the optimal atmospheric duct parameters could not be iterated. (3) The inversion result of the algorithm was the equivalent profile on the AIS signal propagation path, which differed from the actual atmospheric environment.

To compare and verify the differences in the atmospheric environment at different times and directions, the AIS data at 5:00 and 290° were used for atmospheric duct parameter inversion. The inversion results are shown in Figure 22.

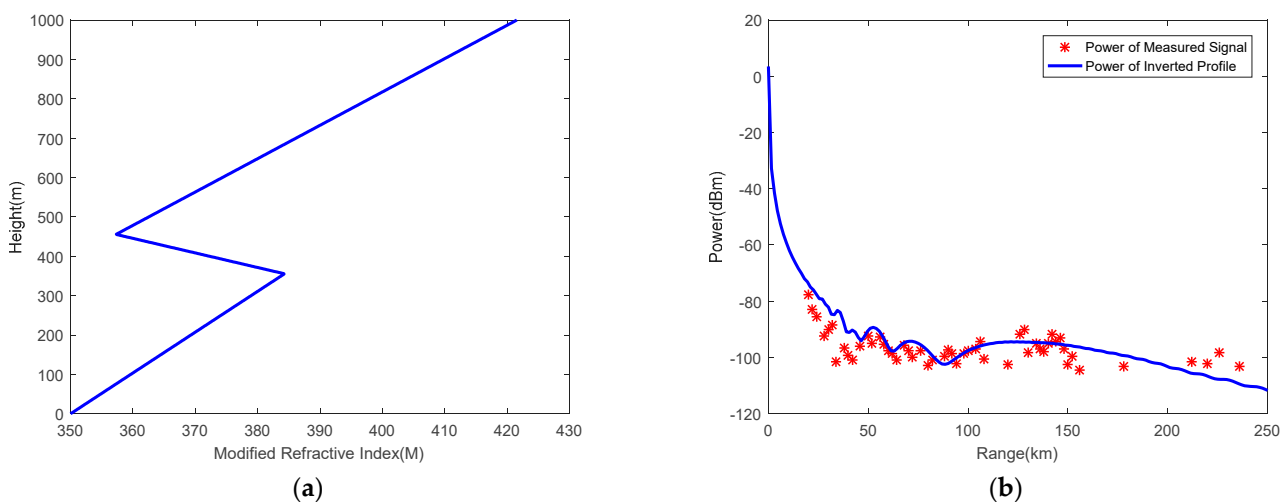


Figure 22. Inversion results using AIS measured data at 5:00 and 290°. (a) Inverted atmospheric duct profile; (b) comparison of measured signal power and inverted profile calculation power.

As shown in Figure 22a, a strong lower atmospheric duct occurred at this time and direction. The slope of the bottom layer is 0.096 M/m, the bottom height of the duct layer is 355.6 m, the thickness of the duct layer is 100 m, and the duct strength is 27 M. As shown in Figure 22b, the inversion power at this time is also consistent with the AIS-measured power. Additionally, the lower atmospheric duct parameters retrieved at this time differ from those retrieved at 19:00.

5. Conclusions

Based on the AIS signal propagation characteristics and PE model, this study compared and analyzed the inversion results of three intelligent optimization algorithms, namely, GA, SA, and PSO, using a simulated atmospheric duct environment. The results indicate that the PSO algorithm exhibits the best inversion effect. The inversion results of the SAPSO and PSO algorithms under different inversion parameters were analyzed statistically. The results indicate that as the number of calculations in the inversion algorithm increases, its results improve, but this trend gradually becomes slower. Therefore, when using AIS data to invert the atmospheric duct parameters, optimization algorithms, iteration times, and population sizes should be selected based on the accuracy requirements of the inversion results and limitations of inversion time. Finally, the atmospheric duct parameters were inverted using the SAPSO algorithm based on the measured AIS data. The calculated power of the inverted profile was consistent with the measured power of the AIS, verifying the reliability of the inversion method.

Owing to the inherent relationship between the parameters of the atmospheric duct, a statistical analysis of atmospheric duct parameters can be conducted based on historical environmental data to obtain the correlation between atmospheric duct parameters, optimize the selection of atmospheric duct parameters during inversion iterations, and improve the efficiency and accuracy of inversion algorithms.

Author Contributions: Conceptualization, C.-G.L. and Z.-P.W.; methodology, H.-G.W., L.-F.H. and L.-J.Z.; software, L.-F.H. and L.-J.Z.; validation, L.-F.H. and Z.-P.W.; formal analysis, C.-G.L. and H.-G.W.; investigation, H.-G.W., L.-F.H. and L.-J.Z.; resources, C.-G.L. and Q.-L.Z.; data curation, J.H. and L.-F.H.; writing—original draft preparation, L.-F.H. and L.-J.Z.; writing—review and editing, Z.-P.W., M.-C.S. and C.-G.L.; visualization, L.-F.H. and L.-J.Z.; supervision, Z.-P.W. and Q.-L.Z.; project administration, C.-G.L. and Q.-L.Z.; funding acquisition, H.-G.W. and M.-C.S. All authors have read and agreed to the published version of the manuscript.

Funding: This research was funded by the National Natural Science Foundation of China (grant number 42076195) and Academician Foundation of Zhang Minggao.

Institutional Review Board Statement: Not applicable.

Informed Consent Statement: Not applicable.

Data Availability Statement: Not applicable.

Acknowledgments: We thank all the editors and reviewers for their valuable comments that greatly improved the presentation of this paper.

Conflicts of Interest: The authors declare that they have no conflict of interest.

References

1. Sirkova, I.; Mikhalev, M. Parabolic wave equation method applied to the tropospheric ducting propagation problem: A survey. *Electromagnetics* **2006**, *26*, 155–173. [[CrossRef](#)]
2. Sirkova, I. Duct occurrence and characteristics for Bulgarian Black Sea shore derived from ECMWF data. *J. Atmos. Sol. Terr. Phys.* **2015**, *135*, 107–117. [[CrossRef](#)]
3. Han, J.; Wu, J.J.; Zhang, L.J.; Wang, H.G.; Zhu, Q.L.; Zhang, C.; Zhao, H.; Zhang, S.B. A classifying-inversion method of offshore atmospheric duct parameters using AIS data based on artificial intelligence. *Remote Sens.* **2022**, *14*, 3197. [[CrossRef](#)]
4. Liu, X.Z.; Wu, Z.S.; Wang, H.G. Inversion method of regional range-dependent surface ducts with a base layer by Doppler weather radar echoes based on WRF model. *Atmosphere* **2020**, *11*, 754. [[CrossRef](#)]
5. Compaleo, J.; Yardim, C.; Xu, L. Refractivity-from-clutter capable, software-defined, coherent-on-receive marine radar. *Radio Sci.* **2021**, *56*, RS007173. [[CrossRef](#)]
6. Brooks, I.M.; Goroch, A.K.; Rogers, D.P. Observations of strong surface radar ducts over the Persian Gulf. *J. Appl. Meteorol.* **1999**, *38*, 1293–1310. [[CrossRef](#)]
7. Saeger, J.T.; Grimes, N.G.; Rickard, H.E.; Hackett, E.E. Evaluation of simplified evaporation duct refractivity models for inversion problems. *Radio Sci.* **2015**, *50*, 1110–1130. [[CrossRef](#)]
8. Kaissassou, S.; Lenouo, A.; Tchawoua, C.; Lopez, P.; Gaye, A.T. Climatology of radar anomalous propagation over West Africa. *J. Atmos. Sol. Terr. Phys.* **2015**, *123*, 1–12. [[CrossRef](#)]

9. Patterson, W.L. *Climatology of Marine Atmospheric Refractive Effects. A Compendium of the Integrated Refractive Effects Prediction System (IREPS) Historical Summaries*; Naval Ocean Systems Center: San Diego, CA, USA, 1982.
10. Babin, S.M. Surface duct height distributions for Wallops Island, Virginia, 1985–1994. *J. Appl. Meteorol. Climatol.* **1996**, *35*, 86–93. [[CrossRef](#)]
11. Mentés, Ş.; Kaymaz, Z. Investigation of surface duct conditions over Istanbul, Turkey. *J. Appl. Meteorol. Climatol.* **2007**, *46*, 318–337. [[CrossRef](#)]
12. Karimian, A.; Yardim, C.; Gerstoft, P.; Hodgkiss, W.S.; Barrios, A.E. Refractivity estimation from sea clutter: An invited review. *Radio Sci.* **2011**, *46*, 1–16. [[CrossRef](#)]
13. Anderson, K.D. Inference of refractivity profiles by satellite-to-ground RF measurements. *Radio Sci.* **1982**, *17*, 653–663. [[CrossRef](#)]
14. Anderson, K.D. Tropospheric refractivity profiles inferred from low elevation angle measurements of Global Positioning System (GPS) signals. In *Propagation Assessments in Coastal Environments*; y Canada Communication Group: Hull, QC, Canada, 1994.
15. Lin, L.K.; Zhao, Z.W.; Zhang, Y.R.; Zhu, Q.L. Tropospheric refractivity profiling based on refractivity profile model using single ground-based global positioning system. *IET Radar Sonar Navig.* **2011**, *5*, 7–11. [[CrossRef](#)]
16. International Telecommunication Union. *Recommendation ITU-R M.1371-5: Technical Characteristics for an Automatic Identification System Using Time-Division Multiple Access in the VHF Maritime Mobile Frequency Band*; ITU: Geneva, Switzerland, 2014; pp. 1371–1375.
17. International Telecommunication Union. *Report M.2123-0: Long Range Detection of Automatic Identification System (AIS) Messages under Various Tropospheric Propagation Conditions*; ITU: Geneva, Switzerland, 2007; p. 2123.
18. Sirkova, I. Automatic Identification System Signals propagation in troposphere ducting conditions. In Proceedings of the IEEE International Black Sea Conference on Communications and Networking (BlackSeaCom), Sofia, Bulgaria, 6–9 June 2022; pp. 331–335. [[CrossRef](#)]
19. Zhang, L.J.; Wang, H.G.; Li, J.R.; Zhang, C.; Han, J.; Wang, Q.N.; Zhu, Q.L. Experimental analysis of lower atmospheric duct monitoring based on AIS signal. *Chin. J. Radio Sci.* **2023**, *38*, 108–113. (In Chinese) [[CrossRef](#)]
20. Tang, W.L.; Cha, H.; Wei, M.; Tian, B. Estimation of surface-based duct parameters from automatic identification system using the Levy flight quantum-behaved particle swarm optimization algorithm. *J. Electromagn. Waves Appl.* **2019**, *33*, 827–837. [[CrossRef](#)]
21. Pastore, D.M.; Greenway, D.P.; Stanek, M.J.; Wessinger, S.E.; Haack, T.; Wang, Q.; Hackett, E.E. Comparison of atmospheric refractivity estimation methods and their influence on radar propagation predictions. *Radio Sci.* **2021**, *56*, RS007244. [[CrossRef](#)]
22. Skolnik, M.I. *RADAR Systems*; McGraw-Hill: New York, NY, USA, 2001.
23. Sirkova, I. Brief review on PE method application to propagation channel modeling in sea environment. *Open Eng.* **2012**, *2*, 19–38. [[CrossRef](#)]
24. Wagner, M.; Gerstoft, P.; Rogers, T. Estimating refractivity from propagation loss in turbulent media. *Radio Sci.* **2016**, *51*, 1876–1894. [[CrossRef](#)]
25. International Telecommunication Union. *Recommendation ITU-R P.341-5: The Concept of Transmission Loss for Radio Links*; ITU: Geneva Switzerland, 2019.
26. International Telecommunication Union. *Recommendation P.525: Calculation of Free-Space Attenuation*; ITU: Geneva, Switzerland, 2019.
27. Palmer, A.J.; Baker, D.C. A novel simple semi-empirical model for the effective earth radius factor. *IEEE Trans. Broadcast.* **2006**, *52*, 557–565. [[CrossRef](#)]
28. Holland, J. *Adaptation in Natural and Artificial Systems*; University of Michigan Press: Ann Arbor, MI, USA, 1975.
29. Goldberg, D. *Genetic Algorithms in Search, Optimization, and Machine Learning*; Addison-Wesley: Boston, MA, USA, 1989.
30. Frenzel, J.F. Genetic algorithms. *IEEE Potentials* **1993**, *12*, 21–24. [[CrossRef](#)]
31. Li, T.; Cui, D.W. Genetic algorithm selection and parameter setting based on rule induction. *Comput. Eng.* **2010**, *36*, 218–223. (In Chinese) [[CrossRef](#)]
32. Metropolis, N.; Rosenbluth, A.W.; Rosenbluth, M.N.; Teller, A.H.; Teller, E. Equation of state calculations by fast computing machines. *J. Chem. Phys.* **1953**, *21*, 1087–1092. [[CrossRef](#)]
33. Yan, L.J.; Li, Z.B.; Wei, J.H. Study on parameter setting method for simulated annealing algorithm. *J. Syst. Simul.* **2008**, *20*, 245–247. (In Chinese)
34. Kennedy, J.; Eberhart, R. Particle swarm optimization. In Proceedings of the IEEE International Conference on Neural Networks, Perth, Australia, 27 November–1 December 1995; pp. 1942–1948. [[CrossRef](#)]
35. Shi, Y.; Eberhart, R.C. A modified particle swarm optimizer. In Proceedings of the IEEE International Conference on Evolutionary Computation, Anchorage, AK, USA, 4–9 May 1998; pp. 69–73. [[CrossRef](#)]
36. Yang, W.; Li, Q.Q. Survey on particle swarm optimization on algorithm. *Eng. Sci.* **2004**, *6*, 87–94. (In Chinese)
37. Zhou, J.; Chen, J.H.; Liu, G.X.; Xu, W.L. Summary on inertia weight in particle swarm optimization Algorithm. *Guangdong Electr. Power* **2013**, *26*, 6–12. (In Chinese) [[CrossRef](#)]

Disclaimer/Publisher’s Note: The statements, opinions and data contained in all publications are solely those of the individual author(s) and contributor(s) and not of MDPI and/or the editor(s). MDPI and/or the editor(s) disclaim responsibility for any injury to people or property resulting from any ideas, methods, instructions or products referred to in the content.